Repulsive hydration forces between calcite surfaces and their effect on the brittle strength of calcite-bearing rocks

Anja Røyne[1], Kim N. Dalby[2], and Tue Hassenkam[2]

[1]Physics of Geological Processes, Department of Physics, University of Oslo, Oslo, Norway, [2]Nano-Science Center, Department of Chemistry, University of Copenhagen, Copenhagen, Denmark

Abstract The long-term mechanical strength of calcite-bearing rocks is highly dependent on the presence and nature of pore fluids, and it has been suggested that the observed effects are due to changes in nanometer-scale surface forces near fracture tips and grain contacts. In this letter, we present measurements of forces between two calcite surfaces in air and water-glycol mixtures using the atomic force microscope. We show a time- and load-dependent adhesion at low water concentrations and a strong repulsion in the presence of water, which is most likely due to hydration of the strongly hydrophilic calcite surfaces. We argue that this hydration repulsion can explain the commonly observed water-induced decrease in strength in calcitic rocks and single calcite crystals. Furthermore, this relatively simple experimental setup may serve as a useful tool for analyzing surface forces in other mineral-fluid combinations.

1. Introduction

The long-term brittle strength of rocks is ultimately controlled by the nanoscale adhesion of grain boundaries and fracture thresholds of single crystals. When macroscopic strain rates are small, kinetic processes on the mineral interface scale give rise to observable subcritical fracture growth, cataclastic compaction, and brittle creep [*Amitrano and Helmstetter*, 2006]. Ample experimental evidence points to a strong dependence of these time-dependent brittle processes on environmental conditions such as humidity, temperature, and pore fluid chemistry [*Brantut et al.*, 2013; *Atkinson*, 1984]. The decrease in mechanical strength of certain rock types in the presence of water is sometimes referred to as water weakening [*Risnes et al.*, 2005].

The underlying physical mechanism for time-dependent brittle deformation depends on mineralogy. For silicates, the general consensus is that hydrolysis of strained Si-O bonds at the crack tip drives subcritical crack growth in humid conditions [*Michalske and Freiman*, 1982]. In the case of mica, where the prominent cleavage along a single plane makes it relatively easy to study single-fracture propagation, experiments and theoretical models suggest that lowering of the surface energy through water adsorption controls the fracture velocity and the threshold for fracture propagation [*Wan et al.*, 1990a]. This mechanism acts in the confined fluid region some distance *behind the crack tip*, and the crack tip region is thought to be too narrow for water molecules to enter. On the other hand, the stress corrosion mechanism for silicates assumes a more open crack tip structure where the water weakening mechanism takes place *at the crack tip* itself. Stress-enhanced dissolution ("true" stress corrosion) is another mechanism that has been suggested to act *at the crack tip* [*Atkinson*, 1984]. For minerals other than mica and silicates, the dominant mechanisms for kinetic fracture propagation are still largely unknown.

Calcite (CaCO$_3$) is a brittle mineral with prominent cleavage along three nonorthogonal planes (10$\bar{1}$4). Calcite is moderately soluble in geologically relevant fluids, and it may deform plastically at moderate loads and temperatures. Time-dependent deformation of calcitic rocks may therefore take place through a combination of brittle (intergranular and intragranular fracture propagation), chemical (dissolution and reprecipitation), and plastic (twinning and dislocation creep) mechanisms, something which complicates the analysis of deformation experiments on calcite-bearing rocks [*Croizé et al.*, 2013]. Calcite is the main component in chalk, which is an important reservoir rock that is severely affected by compaction and subsidence after water injection [*Risnes et al.*, 2005]. Pore fluids are also thought to play an important role in earthquake sequences hosted in carbonate rocks [*Violay et al.*, 2013].
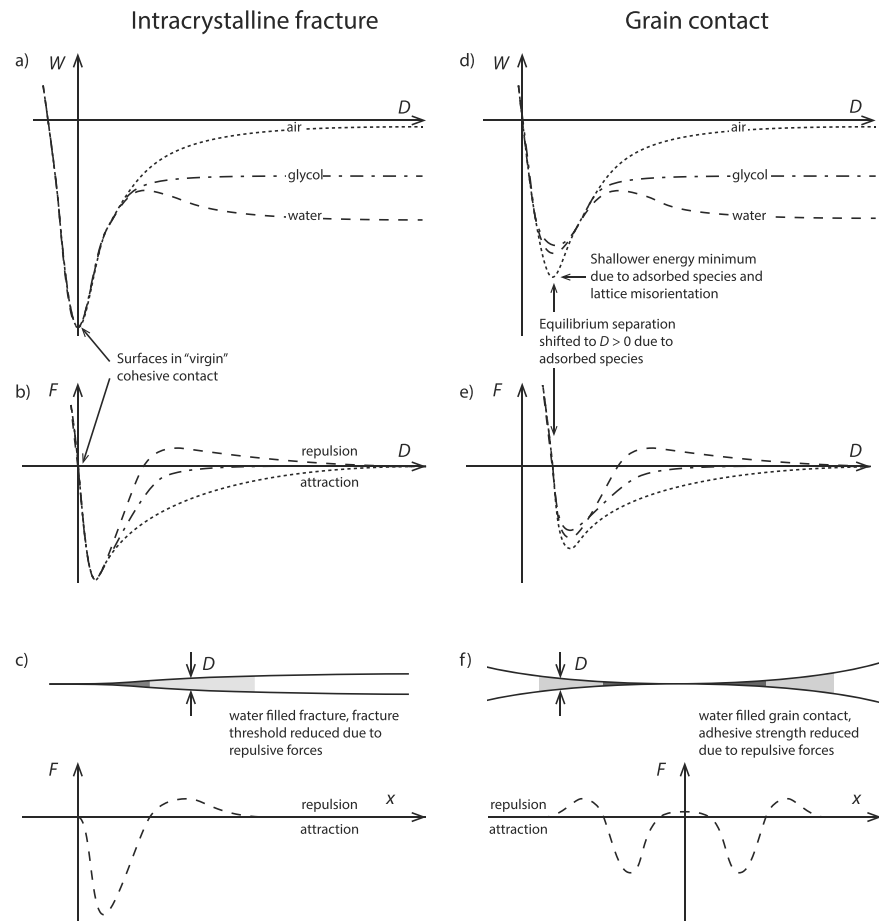
Figure 1. Conceptual sketch of the effect of fluids on the energy W (Figures 1a and 1d) and surface force $F = dW/dD$ (Figures 1b and 1e) as a function of surface separation D or lateral position x in calcite-bearing rocks exposed to air, glycol, or water. $W = 0$ corresponds to the energy of two isolated surfaces in vacuum. (a and b) Separation of two surfaces from "virgin" cohesive contact. On separation in air, the energy gradually increases until it reaches a surface energy that is slightly lower than the vacuum value due to adsorption of water vapor. The surface energy in glycol is lower due to the screening of long-range attractive forces in the fluid medium. The strong thermodynamic driving force for water adsorption on the calcite surface causes a reduction in energy and a repulsive force for separation in water at the distance where one layer of water molecules is adsorbed. (c) Surface forces acting in the near-tip region of a water-filled intracrystalline fracture. Attractive forces operate in the region closest to the crack tip (dark grey), while the strong affinity of water to the fracture surfaces creates a repulsion further away from the tip (light grey). (d and e) Force and energy in a grain contact. The adhesive minimum is smaller due to lattice misorientation and adsorbed chemical species. The energy minimum is shifted to $D > 0$, corresponding to the size of the adsorbed species. (f) Water-filled grain contact. The stress in the center of the contact region is compressive, as predicted by the JKR theory. Attractive forces dominate near the edge of the contact (dark grey), while the presence of water creates a repulsive region (light grey) further out, reducing the total strength of the contact.

Several recent experimental studies suggest that the repulsive forces acting *behind the crack tip*, resulting either from double-layer repulsion or from adsorption of water on calcite surfaces (see next section), are the dominant mechanism for the observed water weakening [*Risnes et al.*, 2005; *Røyne et al.*, 2011; *Rostom et al.*, 2012; *Liteanu et al.*, 2013; *Megawati et al.*, 2013]. In order to study the effect of water activity on the strength of chalk, *Risnes et al.* [2005] used mixtures of water and ethylene glycol. These fluids are fully miscible, allowing the water concentration to be varied without the additional capillary forces that would occur in air-water or oil-water systems. The mechanical effect of ethylene glycol had previously been found to be similar to that of oil. Following the same reasoning, *Røyne et al.* [2011] used water-glycol mixtures in subcritical fracture experiments on single calcite crystals. Both studies found the strength or fracture threshold to decrease with increasing concentration of water and attributed this effect to a repulsive force between the calcite surfaces caused by water adsorption.
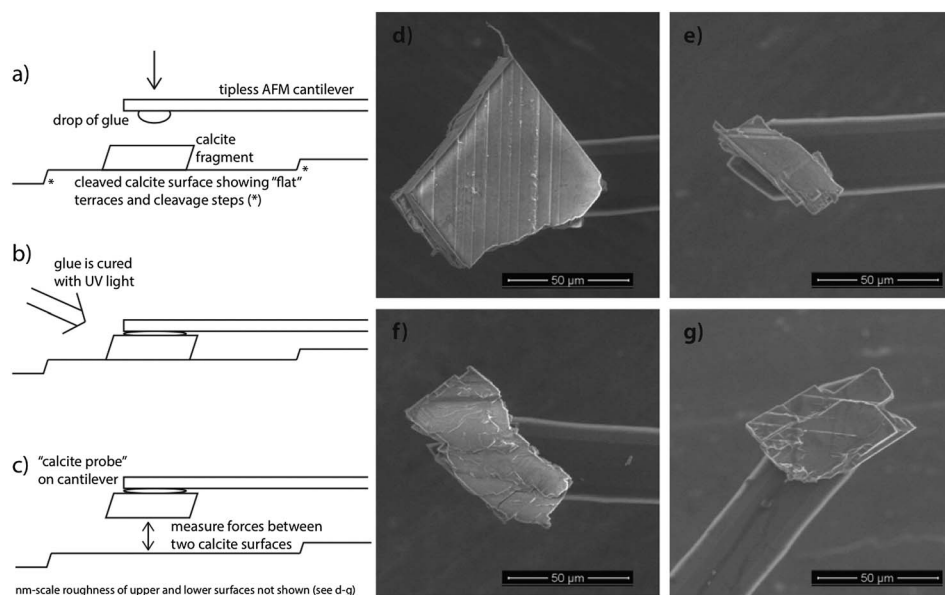
Figure 2. Experimental procedure. (a) Calcite particle resting on a cleaved calcite surface. A drop of UV-curing glue has been picked up by a tipless cantilever, which is gradually lowered onto the particle. (b) While in contact at a set deflection value, the glue is exposed to UV light and cured. (c) Experiments are performed in place by raising and lowering the particle. Fluid is added with the particle in the raised position. Not moving the cantilever-particle assembly ensures that the surfaces stay parallel. (d–g) SEM images of particles on cantilevers. The total area and RMS roughness of these surfaces are 3560 μm^2 and 195 nm (Figure 2d); 317 μm^2 and 73 nm (Figure 2e); 2090 μm^2 and 586 nm (Figure 2f); and 1660 μm^2 and 113 nm (Figure 2g). In Figure 2d, the typical step height is on the order of 10 nm.

The aim of this letter is to test the hypothesis that there exists a strongly repulsive force acting between calcite surfaces in the presence of water, caused by water adsorption. We simplify the system by eliminating the fracture tip and multiple grain contacts from previous experiments and use atomic force microscopy (AFM) to measure the nanometer-scale forces between two calcite surfaces submerged in mixtures of water and glycol. In agreement with the hypothesis, we find a strong repulsion between calcite surfaces in water, while increasing the glycol concentration makes the surfaces adhere to each other.

2. Surface Forces and Fracture Thresholds

The surface energy γ_e of a solid in a given medium e is defined as half the work W required to separate two surfaces, determined by the surface forces F as a function of surface separation D:

$$2\gamma_e \equiv W(\infty) = \int_0^\infty F(D)\mathrm{d}D. \qquad (1)$$

The nanometer-scale forces between mineral surfaces in aqueous solutions are, for separations above a few nanometers and for ionic concentrations less than about 0.1 M, well described by DLVO theory (named after *Derjaguin and Landau* [1941] and *Verwey and Overbeek* [1948]), which includes the van der Waals and electric double-layer forces. Specific ion effects and forces related to the discrete molecular nature of the fluid and surfaces become significant on shorter separations and are often of larger magnitude than the DLVO forces [*Alcantar et al.*, 2003].

In the Griffith theory of brittle fracture, the lower threshold for crack propagation is defined as the point at which the elastic energy released upon incremental fracture propagation, G, is equal to the energy of the two newly created surfaces, $G_0 = 2\gamma_e$. In an atomistic model of the crack tip, the motion of a crack as the loading deviates from the stationary state ($G \neq 2\gamma_e$) is controlled by fluctuation-driven forward and backward jumps, with energy barriers that depend on γ_e and G, giving the following function for the fracture velocity v:

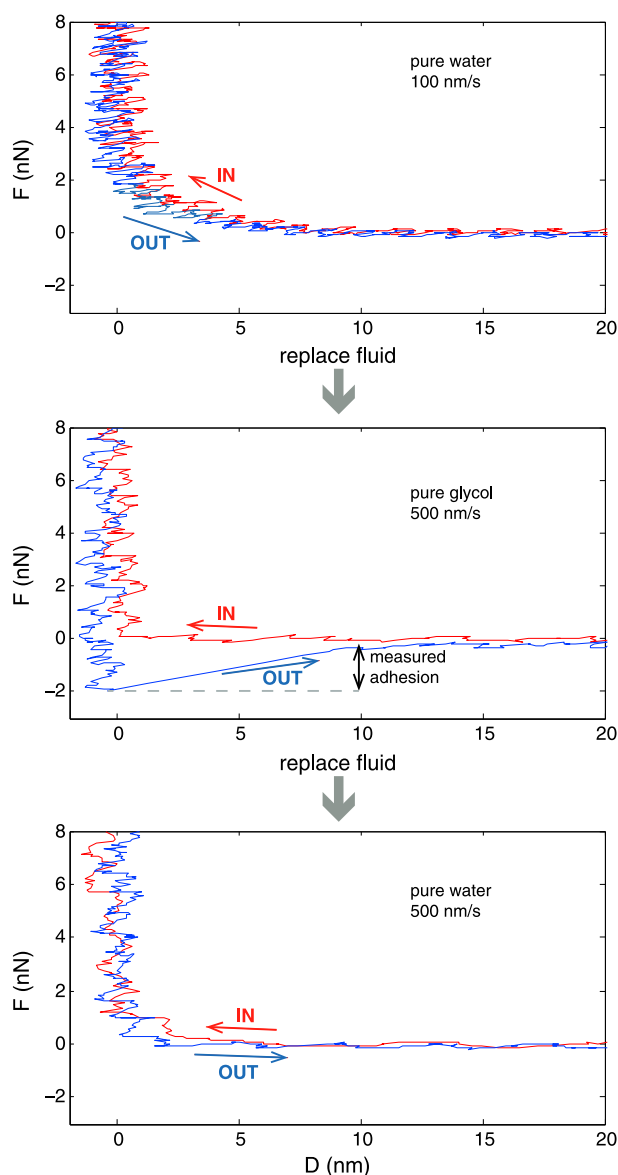$$v = C\sinh\left\{\frac{\alpha(G - G_0)}{kT}\right\} \qquad (2)$$

Figure 3. Force curves measured using a single set of surfaces in water, glycol, and water again. In-runs are plotted as red lines, while out-runs are plotted in blue. A slight long-range repulsion out to approximately 5 nm is seen in the top and bottom panels. The measurements in glycol show a characteristic jump-out of adhesive contact. Small-scale fluctuations in the force curves are due to experimental noise (data sets: 131024-0055, 0066, and 0068).

where C is a material constant and α is an activation area [*Rice*, 1978; *Wan et al.*, 1990b]. For a system originally in equilibrium, a change in fluid chemistry may change the $F(D)$-curve and thereby the threshold load G_0, causing previously stationary fractures to propagate or heal.

The strength of chalk is, at least in part, controlled by the adhesive contacts between micrometer-sized fragments of biomineralized calcite (see Figures 1d–1f). To the first approximation, the Johnson-Kendall-Roberts (JKR) model gives the area of contact and the critical tensile force required to separate two surfaces from adhesive contact as functions of the surface energy γ_e [*Persson*, 2000]. When the fluid chemistry is changed, the corresponding change in γ_e will cause the area of contact to change until it is at equilibrium with the new environment [*Alcantar et al.*, 2003]. Analogous to fracture propagation, the healing or separation of grain contacts can also be viewed as thermally activated processes, causing contacts to strengthen or separate with time, depending on fluid chemistry and applied load.

3. Experimental Setup

The experimental setup is outlined in Figure 2. A piece of optical quality Iceland spar is glued to a microscope slide and cleaved immediately prior to the experiment. The detached part of the crystal is scratched with a scalpel, making a number of fragments land on the cleaved surface. A suitable fragment (between 20 and 50 μm in size, resting on a flat terrace of the cleavage surface) is identified in the microscope. The sample is then placed in the AFM (Asylum MFP-3D), and the calcite fragment is glued (UV-curing Casco Glaslim) to a tipless cantilever (All In One-Al-TL, 15 kHz, 0.2 N/m or 350 kHz, 40 N/m; the stiffer cantilever is used to apply high loads but gives poor resolution of adhesion force). Force measurements are performed by moving the upper surface vertically while monitoring deflection of the cantilever. All measurements are performed in the same position to ensure that the surfaces remain parallel. Preliminary measurements are made to reveal improper curing of glue or small particles trapped between the surfaces. Force runs in fluids are performed at a slow approach velocity to avoid hydrodynamic effects. Hold times in contact range from zero to approximately 1 h, but long hold times give unreliable results due to evaporation and thermal drift.

The solutions used are mixtures of Milli-Q water and ethylene glycol with water volume fractions of 0, 0.25, 0.5, 0.75, and 1.0, all presaturated with $CaCO_3$. A drop of solution is introduced using a long needle syringe.
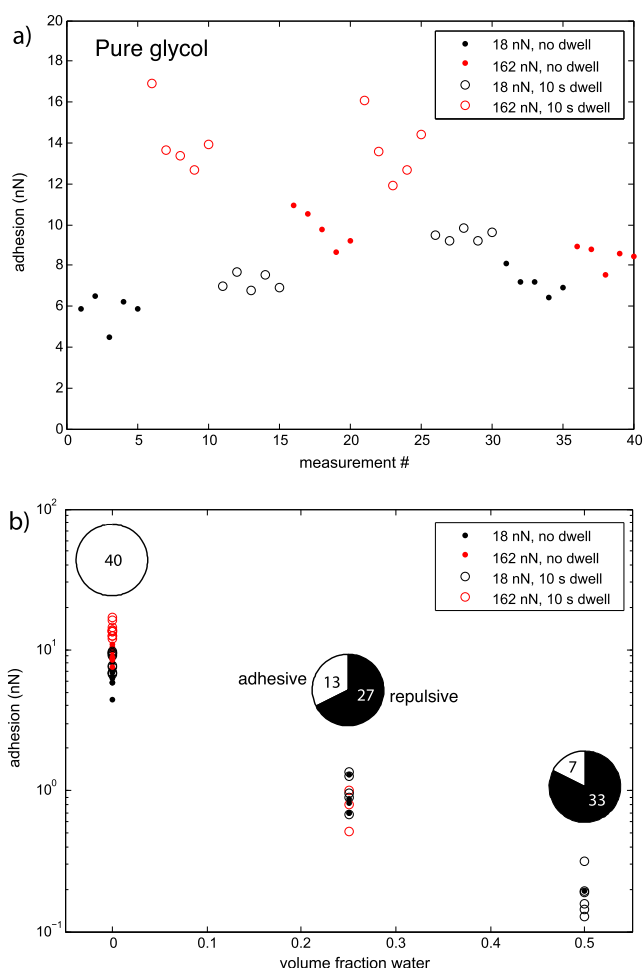
Figure 4. (a) Measured adhesion values for 40 consecutive force runs in pure glycol. Black circles and red squares denote low and high applied loads; filled and open symbols denote zero or 10 s hold time at contact (data sets: 140115-0007–0047). (b) Measured adhesion values for the same set of surfaces in water-glycol mixtures with volumetric water fractions of 0, 0.25, and 0.5 applied in increasing order of water concentration. No adhesion was measured in 0.75 water solution. The pie diagrams show the number of adhesive runs (white) and repulsive runs (black). Note that the adhesion axis is logarithmic. The particle used in this experiment is shown in Figure 2f (data sets: 140115-0007–0129).

Solutions are exchanged by repeatedly wicking out old solution and injecting new. The number of possible fluid exchanges is limited by the risk of the capillary forces pulling the fragment off the cantilever or the introduction of small particles between the surfaces.

The system is equilibrated for at least 10 min after fluid exchange. At the end of each experiment, the cantilever-particle assembly is rinsed with Milli-Q water, dried off, and stored in ambient conditions. The particles are later imaged in the scanning electron microscope (SEM, FEI Quanta 3D), and their surface topography is measured using vertical scanning interferometry (Wyko NT1100).

4. Results

Our results fall into two categories: adhesive and repulsive interactions (Figure 3). Interactions in air and in pure glycol are *always* adhesive, while interactions in pure water are *always* repulsive, regardless of applied force and hold time.

In fluid conditions, a long-range repulsive interaction is sometimes detected a few nanometers before contact (Figure 3).

For any given set of surfaces, the variation in measured adhesion in air is less than 10% when outlying values (attributed to capillary condensation between the surfaces) are ignored. In fluid conditions, adhesion values

vary by up to 2 orders of magnitude, in spite of identical experimental parameters. The adhesion in pure glycol is between 1 and 2 orders of magnitude lower than in air.

In pure glycol and in mixed glycol-water solutions, the measured adhesion increases with both applied force and hold time (Figure 4a).

In mixed solutions, the fraction of adhesive measurements, as well as the average value of the measured adhesion, decreases with increasing water concentration (Figure 4b), irrespective of the order by which fluids are introduced.

5. Discussion

In agreement with our hypothesis, we observe a strong repulsive interaction between calcite surfaces in the presence of water. To establish whether the magnitude of the double-layer repulsion in water is large enough to prevent the surfaces from coming into adhesive contact or whether some other short-range force is needed to explain this observation, we can use DLVO theory in the weak overlap approximation [*Israelachvili*, 2011]. Using 20 mV as an upper limit for the surface potential of calcite in aqueous solutions [*Wolthers et al.*, 2008], the maximum double-layer repulsive pressure between flat surfaces in calcite-saturated solutions at room temperature (pH 8.6, 0.33 mM $CaCO_3$) is 2.8 kPa.

Estimated from SEM images, the areas of the particles used range between 300 and 3500 μm^2. The maximum applied force is 0.16 and 7.0 μN for the soft and the stiff cantilever, respectively. Normalized by the surface area, this corresponds to average pressures up to 540 Pa and 23.3 kPa, which implies that the repulsive interaction we observe at high applied force cannot be due to double-layer repulsion. Instead, it is most likely caused by the repulsive barrier created by hydration of the highly hydrophilic calcite surfaces (Figures 1c and 1d), in agreement with the hypothesis of water weakening due to water adsorption [*Risnes et al.*, 2005; *Røyne et al.*, 2011]. The charge distribution of the (10$\bar{1}$4) cleavage surface of calcite (which is the only crystal face exposed in cleaved samples) is particularly favorable for adsorbed water molecules, something which makes this surface unusually hydrophilic [*Ricci et al.*, 2013]. The adsorbed water molecules are what prevents the surfaces from reaching adhesive contact.

A repulsive hydration force is consistent with the near 50% reduction in surface energy of calcite in water found in a previous subcritical fracture experiment [*Røyne et al.*, 2011]. The integral (equation (1)) of the double-layer repulsion is at least 2 orders of magnitude lower than the surface energy of dry calcite and would therefore only reduce the fracture threshold by a negligible amount. Double-layer repulsion has also been argued to be of insufficient magnitude to account for subcritical fracturing in mica [*Clarke et al.*, 1986; *Chan et al.*, 1986; *Thomson*, 1990; *Wan et al.*, 1990a].

Previous experiments [*Sand et al.*, 2010] have shown that a layer of ethanol remains on a calcite surface when an ethanol solution is exchanged with water. On the contrary, our experiments show that water can completely remove ethylene glycol from the calcite surface. This can be explained by differences in molecular structure: While the nonpolar tails of ethanol molecules create a hydrophobic layer on the calcite surface [*Sand et al.*, 2010], effectively preventing access to water, ethylene glycol has one OH group on either end and does not create this effect.

Calcite surfaces are typically not molecularly flat over large areas [*Stipp et al.*, 1994]. The RMS roughness of the small particles we use is on the order of 100 nm or more (Figure 2). The roughness of the lower calcite surface is probably tens of nanometers, corresponding to cleavage steps that are not visible in the optical microscope. This unknown contact topography hinders the direct comparison of forces measured for different surface pairs, and we should instead focus on how the interactions between a given set of surfaces change in response to the fluid conditions.

Nanoscale surface roughness is known to smear out measured forces or to manifest in an additional exponentially decaying repulsive force [*Valtiner et al.*, 2012]. The long-range repulsion we observe (Figure 3) may be a result of surface roughness, double-layer repulsion, or both.

With rough surfaces, we cannot assume that the applied force is distributed as a uniform pressure across the contact region. Instead, there will be a finite number of asperities that come into contact, each subject to a significantly higher pressure than the average value. If we use the Debye length in pure calcite-saturated water, 12 nm, as a cutoff length for measurable surface forces, a reasonable estimate for the actual area

of contact is about 1% of the total surface area. This implies that even for large particles on soft cantilevers, the asperities have been subject to pressures exceeding 4.6 kPa, effectively ruling out double-layer repulsion as the cause for any of the observed short-range repulsive interactions.

The adhesion we measure in this system is expected to be governed by the van der Waals energy, which to the first approximation is proportional to the Hamaker constant A as $\gamma_{vdW} = A/24\pi D_0$, where D_0 is some cutoff distance [*Israelachvili*, 2011]. Using $A_{cac} = 10.1 \times 10^{-20}$ J for the calcite-air-calcite interface [*Bergström*, 1997] and $A_g = 5.72 \times 10^{-20}$ J for glycol [*Raghavan et al.*, 2000], the combining relation $A_{131} \approx (\sqrt{A_{11}} - \sqrt{A_{33}})^2$ [*Israelachvili*, 2011] gives $A_{cgc} = 0.62 \times 10^{-20}$ J for the calcite-glycol-calcite interface. The ratio of adhesion energies in air and glycol should therefore be $\gamma_{vdW}^{air}/\gamma_{vdW}^{glycol} = 16.3$, which is in the range of what we observe. Following the same reasoning, with $A_{cwc} = 1.44 \times 10^{-20}$ J for calcite in water [*Bergström*, 1997], the adhesion in water should be about twice that in glycol, but since the surfaces cannot be forced into adhesive contact, this is never measured. Furthermore, the measured adhesion is always less in water-glycol mixtures than in pure glycol.

With water present, the hydration repulsion acts against bringing asperities into adhesive contact (Figure 1). When rough surfaces are brought into contact under increasing normal load, successive asperities are compressed, resulting in a real area of contact that is proportional to the applied load for a large range of parameters. The mean pressure at the contact points is less sensitive to the applied load [*Persson*, 2006]. The probability of forming an adhesive contact depends on the number of asperities that are forced into contact and on whether the pressure experienced by these asperities is sufficient to overcome the hydration repulsion. If the force needed to bring the surfaces into adhesive contact is an increasing function of water concentration, then the probability of adhesive contact will be higher for low water concentrations, as observed (Figure 4b). This also explains why the average value of the measured adhesion decreases with increasing water concentration.

The highly variable measured adhesion in fluid conditions can be explained by a combination of surface roughness and surface dynamics. Variations in measured adhesion is commonly observed in AFM measurements using macroscopic surfaces of nanoscale roughness and is attributed to structural changes in the contact region [*Farshchi-Tabrizi et al.*, 2006]. Calcite surfaces are highly dynamic in the presence of fluids [*Stipp et al.*, 1994], and we expect asperities to evolve through dissolution and recrystallization over the time scale of our experiments. This likely also explains why the magnitude of the long-range repulsion varies between measurements.

The observed increase in adhesion with contact time (Figure 4a) may be due to dissolution in regions of high normal stress and subsequent precipitation at the edges of asperities. Such growth of contact area for reactive mineral interfaces is thought to be a primary mechanism for fault healing and time-dependent frictional strength [*Renard et al.*, 2012]. Alternatively, a number of asperities that experience a load which is insufficient to push them into instantaneous contact may adhere with time through thermal fluctuations, analogous to the healing of a fracture when $G < G_0$ (equation (2)). This also leads to an increased contact area and hence measured adhesion. However, unlike the first hypothesis, this requires the movement of solvent away from contacts instead of the redistribution of solid material through dissolution and precipitation. At the moment, we have no method for distinguishing between these two mechanisms.

6. Conclusions and Implications

Based on our measurements, we can verify the existence of a high-magnitude, short-range repulsive force between calcite surfaces in water, which can be attributed to water adsorption. This hydration repulsion has previously been postulated to be responsible for water weakening of calcitic rocks and single calcite crystals [*Risnes et al.*, 2005; *Røyne et al.*, 2011], and our results support this hypothesis.

AFM measurements of forces between mineral surfaces allow the effects of surface forces, operating in the thin fluid film behind the crack tip and at grain contacts, to be isolated from possible competing mechanisms such as dissolution creep, dislocation creep, and the development of microfractures in a macroscopic sample. Performing similar experiments under varying fluid conditions therefore presents a new way forward for analyzing the effects of fluid chemistry on the long-term brittle strength of rocks and other polycrystalline materials.

The degree of salinity of pore fluids is known to affect the strength and fracture properties of rocks [*Risnes et al.*, 2003; *Nara et al.*, 2014]. We have previously [*Rostom et al.*, 2012] found single calcite crystals to exhibit a higher fracture threshold in solutions of high ionic strength. This strengthening has been argued to be due to screening of the electric double layers and subsequent disappearance of the double-layer repulsion [*Nara et al.*, 2014] or to the decrease in water activity [*Risnes et al.*, 2005]. Based on our current results, we expect the effect of dissolved ions on the hydration of the calcite surfaces, rather than relatively weak double-layer forces, to be the controlling mechanism. We are currently using the AFM to measure the effect of salinity and specific ions on the forces between calcite surfaces.

References

Alcantar, N., J. Israelachvili, and J. Boles (2003), Forces and ionic transport between mica surfaces: Implications for pressure solution, *Geochim. Cosmochim. Acta*, *67*, 1289–1304, doi:10.1016/s0016-7037(02)01270-x.

Amitrano, D., and A. Helmstetter (2006), Brittle creep, damage, and time to failure in rocks, *J. Geophys. Res.*, *111*, B11201, doi:10.1029/2005JB004252.

Atkinson, B. K. (1984), Subcritical crack growth in geological materials, *J. Geophys. Res.*, *89*, 4077–4114.

Bergström, L. (1997), Hamaker constants of inorganic materials, *Adv. Colloid Interface Sci.*, *70*, 125–169, doi:10.1016/s0001-8686(97)00003-1.

Brantut, N., M. J. Heap, P. G. Meredith, and P. Baud (2013), Time-dependent cracking and brittle creep in crustal rocks: A review, *J. Struct. Geol.*, *52*, 17–43, doi:10.1016/j.jsg.2013.03.007.

Chan, D., B. D. Hughes, and L. R. White (1986), A physically consistent theory of fracture in a brittle solid, *J. Colloid Interface Sci.*, *115*, 240–259.

Clarke, D., B. Lawn, and D. Roach (1986), The role of surface forces in fracture, in *Fracture Mechanics of Ceramics*, vol. 8, edited by D. Clarke, B. Lawn, and D. Roach, pp. 341–350, Plenum, New York.

Croizé, D., F. Renard, and J.-P. Gratier (2013), Compaction and porosity reduction in carbonates: A review of observations, theory, and experiments, *Adv. Geophys.*, *54*, 181–238.

Derjaguin, B., and L. Landau (1941), Theory of the stability of strongly charged lyophobic sols and of the adhesion of strongly charged particles in solutions of electrolytes, *Prog. Surf. Sci.*, *43*, 1–4.

Farshchi-Tabrizi, M., M. Kappl, Y. Cheng, J. Gutmann, and H. J. Butt (2006), On the adhesion between fine particles and nanocontacts: An atomic force microscope study, *Langmuir*, *22*, 2171–84, doi:10.1021/la052760z.

Israelachvili, J. (2011), *Intermolecular and Surface Forces*, 3rd ed., Academic Press, London.

Liteanu, E., C. J. Spiers, and J. H. P. de Bresser (2013), The influence of water and supercritical CO_2 on the failure behavior of chalk, *Tectonophysics*, *599*, 157–169, doi:10.1016/j.tecto.2013.04.013.

Megawati, M., A. Hiorth, and M. Madland (2013), The impact of surface charge on the mechanical behavior of high-porosity chalk, *Rock Mech. Rock Eng.*, *46*, 1073–1090, doi:10.1007/s00603-012-0317-z.

Michalske, T. A., and S. W. Freiman (1982), A molecular interpretation of stress corrosion in silica, *Nature*, *295*, 511–512.

Nara, Y., R. Nakabayashi, M. Maruyama, H. Hiroyoshi, T. Yoneda, and K. Kaneko (2014), Influences of electrolyte concentration on subcritical crack growth in sandstone in water, *Eng. Geol.*, *179*, 41–49.

Persson, B. (2000), *Sliding Friction. Physical Principles and Applications*, 2nd ed., Springer, Berlin.

Persson, B. N. J. (2006), Contact mechanics for randomly rough surfaces, *Surf. Sci. Rep.*, *61*, 201–227, doi:10.1016/j.surfrep.2006.04.001.

Raghavan, S., H. Walls, and S. Khan (2000), Rheology of silica dispersions in organic liquids: New evidence for solvation forces dictated by hydrogen bonding, *Langmuir*, *16*, 7920–7930.

Renard, F., S. Beauprêtre, C. Voisin, D. Zigone, T. Candela, D. K. Dysthe, and J.-P. Gratier (2012), Strength evolution of a reactive frictional interface is controlled by the dynamics of contacts and chemical effects, *Earth Planet. Sci. Lett.*, *341–344*, 20–34, doi:10.1016/j.epsl.2012.04.048.

Ricci, M., P. Spijker, F. Stellacci, J. F. Molinari, and K. Voïtchovsky (2013), Direct visualization of single ions in the Stern layer of calcite, *Langmuir*, *29*, 2207–16, doi:10.1021/la3044736.

Rice, J. R. (1978), Thermodynamics of quasi-static growth of Griffith cracks, *J. Mech. Phys. Solids*, *26*, 61–78.

Risnes, R., H. Haghighi, R. I. Korsnes, and O. Natvik (2003), Chalk-fluid interactions with glycol and brines, *Tectonophysics*, *370*, 213–226.

Risnes, R., M. Madland, M. Hole, and N. Kwabiah (2005), Water weakening of chalk—Mechanical effects of water-glycol mixtures, *J. Pet. Sci. Eng.*, *48*, 21–36, doi:10.1016/j.petrol.2005.04.004.

Rostom, F., A. Røyne, D. K. Dysthe, and F. Renard (2012), Effect of fluid salinity on subcritical crack propagation in calcite, *Tectonophysics*, *583*, 68–75, doi:10.1016/j.tecto.2012.10.023.

Røyne, A., J. Bisschop, and D. K. Dysthe (2011), Experimental investigation of surface energy and subcritical crack growth in calcite, *J. Geophys. Res.*, *116*, B04204, doi:10.1029/2010JB008033.

Sand, K. K., M. Yang, E. Makovicky, D. J. Cooke, T. Hassenkam, K. Bechgaard, and S. L. Stipp (2010), Binding of ethanol on calcite: The role of the OH bond and its relevance to biomineralization, *Langmuir*, *26*, 15239–47, doi:10.1021/la101136j.

Stipp, S. L. S., C. M. Eggleston, and B. S. Nielsen (1994), Calcite surface structure observed at microtopographic and molecular scales with atomic force microscopy (AFM), *Geochim. Cosmochim. Acta*, *58*, 3023–3033.

Thomson, R. (1990), The molecular wedge in a brittle crack: A simulation of mica water, *J. Mater. Res.*, *5*, 524–534.

Valtiner, M., X. Banquy, K. Kristiansen, G. W. Greene, and J. N. Israelachvili (2012), The electrochemical surface forces apparatus: The effect of surface roughness, electrostatic surface potentials, and anodic oxide growth on interaction forces, and friction between dissimilar surfaces in aqueous solutions, *Langmuir*, *28*, 13080–93, doi:10.1021/la3018216.

Verwey, E. J. W., and J. T. G. Overbeek (1948), *Theory of the Stability of Lyophobic Colloids*, Elsevier, Amsterdam.

Violay, M., S. Nielsen, E. Spagnuolo, D. Cinti, G. Di Toro, and G. Di Stefano (2013), Pore fluid in experimental calcite-bearing faults: Abrupt weakening and geochemical signature of co-seismic processes, *Earth Planet. Sci. Lett.*, *361*, 74–84, doi:10.1016/j.epsl.2012.11.021.

Wan, K.-T., N. Aimard, S. Lathabai, R. G. Horn, and B. R. Lawn (1990a), Interfacial energy states of moisture-exposed cracks in mica, *J. Mater. Res.*, *5*, 172–182.

Wan, K.-T., S. Lathabai, and B. R. Lawn (1990b), Crack velocity functions and thresholds in brittle solids, *J. Eur. Ceram. Soc.*, *6*, 259–268.

Wolthers, M., L. Charlet, and P. Van Cappellen (2008), The surface chemistry of divalent metal carbonate minerals: A critical assessment of surface charge and potential data using the charge distribution multi-site ion complexation model, *Am. J. Sci.*, *308*, 905–941, doi:10.2475/08.2008.02.